Pergamon

Int. J. Heat Mass Transfer. Vol. 39, No. 15, pp. 3193–3210, 1996

0017-9310/96 $15.00+0.00

0017-9310(95)00404-1

A combined numerical and experimental study of air convection in a differentially heated rotating cubic cavity

Y. T. KER and T. F. LIN†

Department of Mechanical Engineering, National Chiao Tung University, Hsinchu, Taiwan, Republic of China

(*Received* 23 *August* 1995 *and in final form* 6 *November* 1995)

Abstract—A combined numerical and experimental study was carried out to investigate the steady convective flow structure and the flow stability in an inclined cubic air cavity subject to differential heating across a pair of side walls and subject to rotation about an axis which is normal to the insulated bottom wall and through the geometric center of the cavity. In the numerical simulation the three-dimensional Navier-Stokes and energy equations were directly solved by the projection method for the vertical cavity ($\phi = 0°$). While in the experimental study the air temperature in the cavity at selected locations was detected for both steady and unsteady flows. Results were obtained for $\Delta T = 10°C$ and 4.6°C, Ω from 0 rpm to 453 rpm and ϕ from 0° to 75°. The numerical results clearly revealed the complex multicellular flow structure in a vertical cavity at low rotation rates in which the mutual interactions of the thermal buoyancy, Coriolis force and rotational buoyancy are important. The experimental data suggested that the air flow can be stabilized by the cavity rotation when the rotation rate is low. But at high rotating speed the cavity rotation produced destabilizing effects. Copyright © 1996 Elsevier Science Ltd.

1. INTRODUCTION

This study is motivated by the fact that rotation can exhibit profound influences on the convection in a rotating air cavity subject to differential heating, when the associate Coriolis and centrifugal forces are in comparable magnitudes with the thermal buoyancy. However, the details on how these interactive forces act on the complex resulting flow are still poorly understood. The effects of the centrifugal force, which are often ignored in the literature, need to be accounted for herein, since it can significantly modify the rotating flow of a variable density fluid resulting from the temperature nonuniformity. This is named as the 'rotational buoyancy'. The governing nondimensional groups characterizing the thermal buoyancy, Coriolis force and rotational buoyancy for the rotating air cavity flow under investigation are, respectively, the thermal Rayleigh number Ra ($=\beta g \Delta T H^3/\alpha\nu$), Taylor number Ta ($=\Omega^2 H^4/\nu^2$) and rotational Rayleigh number Ra_w ($=\beta\Omega^2 \Delta T H^4/\nu\alpha$). It is, however, realized that for a cavity of fixed size the flow in it is governed by only two physical parameters—the rotation rate Ω and temperature difference ΔT. This simply indicates that the three nondimensional groups are interdependent and their values can not be arbitrarily assigned. Thus, the parametric study of the flow through numerical simulation in our previous investigation by Lee and Lin [1] can only provide the physics of flow, but is not in accord with the practical situation. In this investigation a combined numerical and experimental study was carried out to explore the temperature difference and rotation rate on the detailed flow and thermal characteristics of the air convection in a cubic cavity. Attention was mainly focused on the steady three-dimensional flow and thermal structures in the numerical simulation. While in the experimental measurement the time variations of the air temperature were measured to provide the data for verifying the numerical results and to study the effects of the rotation on the stability of the flow.

In the literature considerable attention has been paid to the convection in a bottom heated, infinite bounded horizontal layer of fluid rotating at a constant angular speed about a vertical axis [2–8]. From linear stability analysis, Niller and Bisshopp [2] noted that in the limit of a large Taylor number the viscous effects play an important role in a thin layer near the boundary and the critical Rayleigh number Ra_c for the onset of convection is independent of whether the boundaries are rigid or free. Numerical analysis conducted by Veronis [3] indicated that the Prandtl number exhibits significant effects on the flow and thermal structures. For the limit of infinite Prandtl number Küppers and Lortz [4] showed that no stable steady-state convective flow exists if the Taylor number exceeds a certain critical value. Rossby [5] experimentally observed the subcritical instability in a water layer for $Ta > 5 \times 10^4$ and in an air layer for $Ta < 10^5$. In addition, for water at $Ra > 10^4$ the Nusselt number was found to increase with the Taylor number. The

† Author to whom correspondence should be addressed.

NOMENCLATURE

g magnitude of the gravitational acceleration
$\mathbf{g}$ gravitational acceleration
H length of cavity
Nu local Nusselt number
$\overline{Nu}$ space-average Nusselt number
$\overline{Nu_z}$ Y-direction average Nusselt number
P_m motion pressure
Pr Prandtl number
$\mathbf{r}$ position vector
Ra Rayleigh number
Ra_w rotational Rayleigh number
t time
T local temperature
Ta Taylor number
T_H temperature of the hot wall
T_L temperature of the cold wall
T_0 initial fluid temperature, $T_0 = 0.5(T_H + T_L)$
u, v, w dimensional velocities in x, y, z directions
U, V, W dimensionless velocities in X, Y, Z directions
$|U|_{max}, |V|_{max}, |W|_{max}$ maximum dimensionless velocity magnitudes in X, Y, Z directions
$\mathbf{v}$ velocity vector
x, y, z dimensional coordinate systems
X, Y, Z dimensionless coordinate systems.

Greek symbols

α thermal diffusivity
β thermal expansion coefficient
δT amplitude of temperature oscillation
δT_0 amplitude of temperature oscillation for $\phi = 75^\circ$ and $\Omega = 0$ rpm
ΔT temperature difference between the hot and cold walls
θ dimensionless temperature
ν kinematic viscosity
ρ air density at temperature T
ρ_0 air density at temperature T_0
τ dimensionless time
ϕ inclined angle between gravity and rotating axis
Ω magnitude of rotating rate
$\mathbf{\Omega}$ rotating rate.

opposite trend is the case for air. Besides, at a large Taylor number the oscillatory convection is preferred in mercury. Based on the mean-field approximation, Hunter and Riahi [6] analytically showed the non-monotonic variation of the Nusselt number with the Taylor number. Linear stability analysis from Rudraiah and Chandna [7] indicated that the critical Rayleigh number was relatively sensitive to the method and rate of heating, Coriolis force and the nature of the bounding surfaces of the fluid layer. The analysis from Clever and Busse [8] suggests that the critical Rayleigh number for the onset of oscillatory motion is higher for the higher Taylor and Prandtl numbers.

Another geometry of considerable interest is the flow in a bottom heated vertical closed circular cylinder rotating about its axis. Experiments for silicone oil carried out by Hudson and his coworkers [9, 10] indicated that the Nusselt number increases with the rotation rate. Steady axisymmetric numerical simulation was carried out by Chew [11]. The onset of steady natural convection was shown by Buell and Catton [12] to be rather sensitive to the lateral thermal boundary condition. Pfotenhauer *et al.* [13] reported experimental results for the effects of the cylinder geometry on the onset of convection for the low temperature liquid helium. For water subject to the Rayleigh number ranging from 10^6 to 2×10^{11} and Taylor number from 10^6 to 10^{12}, Boubnov and Golitsyn [14] experimentally observed a ring pattern of convective flow resulting from the fluid spin-up and vertex interactions between two adjacent vortices. Kirdyashkin and Distanov [15] found that a periodically changing rotation speed can result in periodical temperature changes throughout the entire liquid layer.

Experimental data for the Nusselt number in a top heated horizontal rectangular cavity of silicone oil rotating about a vertical axis passing through the geometric center of the cavity were presented by Abell and Hudson [16]. Hathaway and Somerville [17] conducted a three-dimensional and unsteady numerical simulation of an inclined rotating layer, with the rotation vector tilted from the vertical. The tilting of the rotation vector was found to produce significant change in the flow structure. A combined theoretical, numerical and experimental study was presented by Bühler and Oertel [18] to investigate thermal convection in rotating rectangular shallow box heated from below. First, linear stability analysis was used to predict the onset of steady and oscillatory convection and three-dimensional flow configuration. Then, the numerical analysis predicted the change of the roll orientation with the Taylor number. Finally, the flow structures at various Rayleigh and Taylor numbers were visualized. Unusual flow circulation was experimentally observed by Condie and Griffiths [19] for a horizontal layer of water.

The above literature review indicates that the early studies mainly focused on the effects of the rotation on the onset of convection and the overall heat transfer at supercritical Rayleigh numbers. The detailed pro-

cesses on how the Coriolis and centrifugal forces affect the convective flow structure and its stability in a differentially heated cavity are still not well understood. In this study, a combined three-dimensional numerical simulation and experimental measurement was carried out to enhance our understanding on the differentially heated rotation cavity flow.

2. MATHEMATICAL MODELING AND SOLUTION METHOD

2.1. *Mathematical model*

The schematic diagram of the physical system under investigation is depicted in Fig. 1 along with the chosen coordinates fixed on the rotating cavity. Initially at time $t < 0$, the cubic cavity and inside air are both stationary and isothermal at T_0. At $t \geqslant 0$ the cavity is rotated at a constant angular speed Ω about an axis which is parallel with the side walls and is through the center of the cavity. Meanwhile, two opposite side walls are suddenly raised and lowered, respectively, to two different, but uniform temperatures $T_0+\Delta T/2$ and $T_0-\Delta T/2$, while the other walls are thermally well insulated. The rotating axis which coincides with the z-axis inclines from the vertically upward direction by an angle ϕ. The inclined angle is in fact the angle between the hot plate and vertically upward direction. Thus, the air flow inside the cavity is simultaneously driven by the rotation and thermal buoyancy. By adopting the generalized Boussinesq approximation [20], in which the linear density variation with the temperature is considered in both the body force and centrifugal force terms, the thermal and rotational buoyancies and Coriolis force acting on the flow are, respectively, equal to $-\rho_0 g\beta(T-T_0)$, $\rho_0\beta(T-T_0)\boldsymbol{\Omega}\times\boldsymbol{\Omega}\times\mathbf{r}$ and $-2\rho_0\boldsymbol{\Omega}\times\mathbf{v}$, where $\mathbf{r}$ is the position vector (x, y, z) defined on the rotating coordinate system. The driven flow in the rotating cavity can be described by the following basic equations:

$$\frac{\partial u}{\partial x}+\frac{\partial v}{\partial y}+\frac{\partial w}{\partial z}=0 \tag{1}$$

$$\frac{\partial u}{\partial t}+u\frac{\partial u}{\partial x}+v\frac{\partial u}{\partial y}+w\frac{\partial u}{\partial z}=-\frac{1}{\rho}\frac{\partial p_m}{\partial x}+\nu\nabla^2 u+2\Omega v-\Omega^2 x\beta(T-T_0)+g\beta(T-T_0)\sin\phi\cdot\cos\Omega t \tag{2}$$

$$\frac{\partial v}{\partial t}+u\frac{\partial v}{\partial x}+v\frac{\partial v}{\partial y}+w\frac{\partial v}{\partial z}=-\frac{1}{\rho}\frac{\partial p_m}{\partial y}+\nu\nabla^2 v-2\Omega u-\Omega^2 y\beta(T-T_0)-g\beta(T-T_0)\sin\Omega\phi\cdot\sin\Omega t \tag{3}$$

$$\frac{\partial w}{\partial t}+u\frac{\partial w}{\partial x}+v\frac{\partial w}{\partial y}+w\frac{\partial w}{\partial z}$$

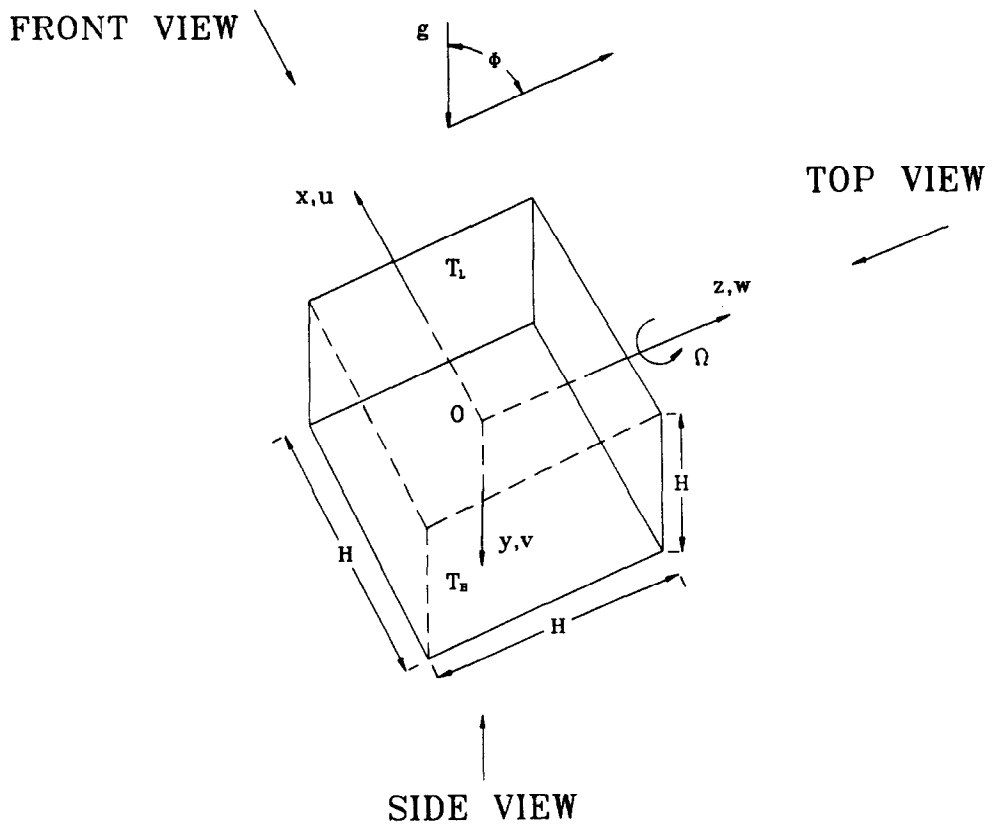

Fig. 1. Schematic diagram of the physical system.

$$= -\frac{1}{\rho}\frac{\partial p_m}{\partial z} + \nu\nabla^2 w + g\beta(T-T_0)\cos\phi \quad (4)$$

$$\frac{\partial T}{\partial t} + u\frac{\partial T}{\partial x} + v\frac{\partial T}{\partial y} + w\frac{\partial T}{\partial z} = \alpha\nabla^2 T \quad (5)$$

where

$$\nabla^2 = \frac{\partial^2}{\partial x^2} + \frac{\partial^2}{\partial y^2} + \frac{\partial^2}{\partial z^2}$$

and p_m is the motion pressure defined as

$$-\frac{\partial p_m}{\partial x} = -\frac{\partial p}{\partial x} + \rho_0\Omega^2 x - \rho_0 g\sin\phi\cdot\cos\Omega t,$$

$$-\frac{\partial p_m}{\partial y} = -\frac{\partial p}{\partial y} + \rho_0\Omega^2 y + \rho_0 g\sin\phi\cdot\sin\Omega t$$

and

$$-\frac{\partial p_m}{\partial z} = -\frac{\partial p}{\partial z} - \rho_0 g\cos\phi.$$

This indicates that the hydrostatic pressure and the centrifugal force acting on the fluid at the referenced density ρ_0 are absorbed in the motion pressure p_m. The three velocity components u, v and w are defined on the coordinates x, y and z rotating with the cavity, as shown in Fig. 1. Note that the third and fourth terms on the right hand side of equations (2) and (3), respectively, denote the momentum change of the flow due to the Coriolis force and the centrifugal force on a variable density fluid subject to temperature nonuniformity. The corresponding initial and boundary conditions are

$$t<0,\quad u=v=w=0 \quad\text{and}\quad T=T_0 \quad \text{for all } x,y,z$$

$$t\geqslant 0,\quad x=\frac{H}{2},\quad u=v=w=0,\quad T=T_0-\frac{\Delta T}{2}$$

$$x=-\frac{H}{2},\quad u=v=w=0,\quad T=T_0+\frac{\Delta T}{2}$$

$$y=\pm\frac{H}{2},\quad u=v=w=0,\quad \frac{\partial T}{\partial y}=0$$

$$z=\pm\frac{H}{2},\quad u=v=w=0,\quad \frac{\partial T}{\partial z}=0. \quad (6)$$

The results from the computation are to be presented in terms of the following nondimensional variables:

$$X=x/H,\quad Y=y/H,\quad Z=z/H,\quad \tau=t/(H^2/\alpha),$$

$$U=u/(\alpha/H),\quad V=v/(\alpha/H),\quad W=w/(\alpha/H)$$

$$\theta=(T-T_L)/\Delta T,\quad P=p_m/(\rho\alpha^2/H^2),\quad Pr=\nu/\alpha$$

$$Ra=g\beta\Delta T H^3/(\nu\alpha),\quad Ra_w=\Omega^2 H\beta\Delta T H^3/(\nu\alpha),$$

$$Ta=\Omega^2 H^4/\nu^2. \quad (7)$$

Note that for the rotating cavity flow $Ra_w = Ra\cdot(\Omega^2 H/g)$ and $Ra_w = Ta\cdot(\beta\Delta T\cdot Pr)$. Also note that the values of $(\beta\cdot Pr)$ for the gas and liquid at the same temperature do not differ significantly. Hence, the rotational buoyancy becomes important for a high rotating speed, large cavity dimension or large temperature difference.

In addition to examining the time evolution of the velocity and temperature fields, results for the local, y-direction average and space-average Nusselt numbers Nu, $\overline{Nu}_z$ and $\overline{Nu}$ on the heated or cooled plates are important in thermal design and can be evaluated from

$$Nu = -\left.\frac{\partial\theta}{\partial X}\right|_{X=\pm 0.5} \quad (8)$$

$$\overline{Nu}_z = \int_{-0.5}^{0.5} Nu\,dY \quad (9)$$

$$\overline{Nu} = \int_{-0.5}^{0.5}\int_{-0.5}^{0.5} Nu\,dY\,dZ. \quad (10)$$

2.2. *Solution method*

The basic equations for the present three-dimensional unsteady rotating cavity flow were solved numerically. In particular, the power-law scheme [21] was used to discretize equations (1)–(5) on a nonuniform staggered grid system with the pressure and temperature defined at the mesh centers. The resulting finite difference equations were solved by the projection method [22]. The detailed solution procedures were described in our earlier work [1].

In view of the complex flow to be simulated, stringent program tests have been conducted to verify the proposed solution method [1]. First, computations were carried out for the limiting case of a nonrotating ($\Omega = 0$) vertical cavity. Our predicted steady local Nusselt numbers for various cases are in good agreement with the results of Bauman *et al.* [23], De Vahl Davis [24], Bajorek and Lloyd [25] and Hamady [26]. Next, tests were performed for a rotating cavity. Our predictions were compared with the experimental data of Hamady [26] with reasonable agreement. Furthermore, results for the transient variation of the space-average Nusselt numbers on the hot wall $\overline{Nu}$ were compared with those from Kuwahara *et al.* [27] for $Ra = 10^4$ and 10^6 in a nonrotating cavity. Good agreement is noted over the entire transient. Good agreement is also noted for other flow and thermal characteristics. Finally, grid-independence tests were conducted for a number of cases. Results from such tests indicated that the differences in the predicted maximum local velocity magnitudes $|U|_{max}$, $|V|_{max}$ and $|W|_{max}$ from the $30\times30\times30$ and $40\times40\times40$ grids are all less than 4.2% during the entire transient. Better agreement is obtained for $\overline{Nu}$. The differences in $\overline{Nu}$ predicted from these two grids are within 1% during the entire transient. Furthermore, comparison of the velocity and temperature profiles also showed good

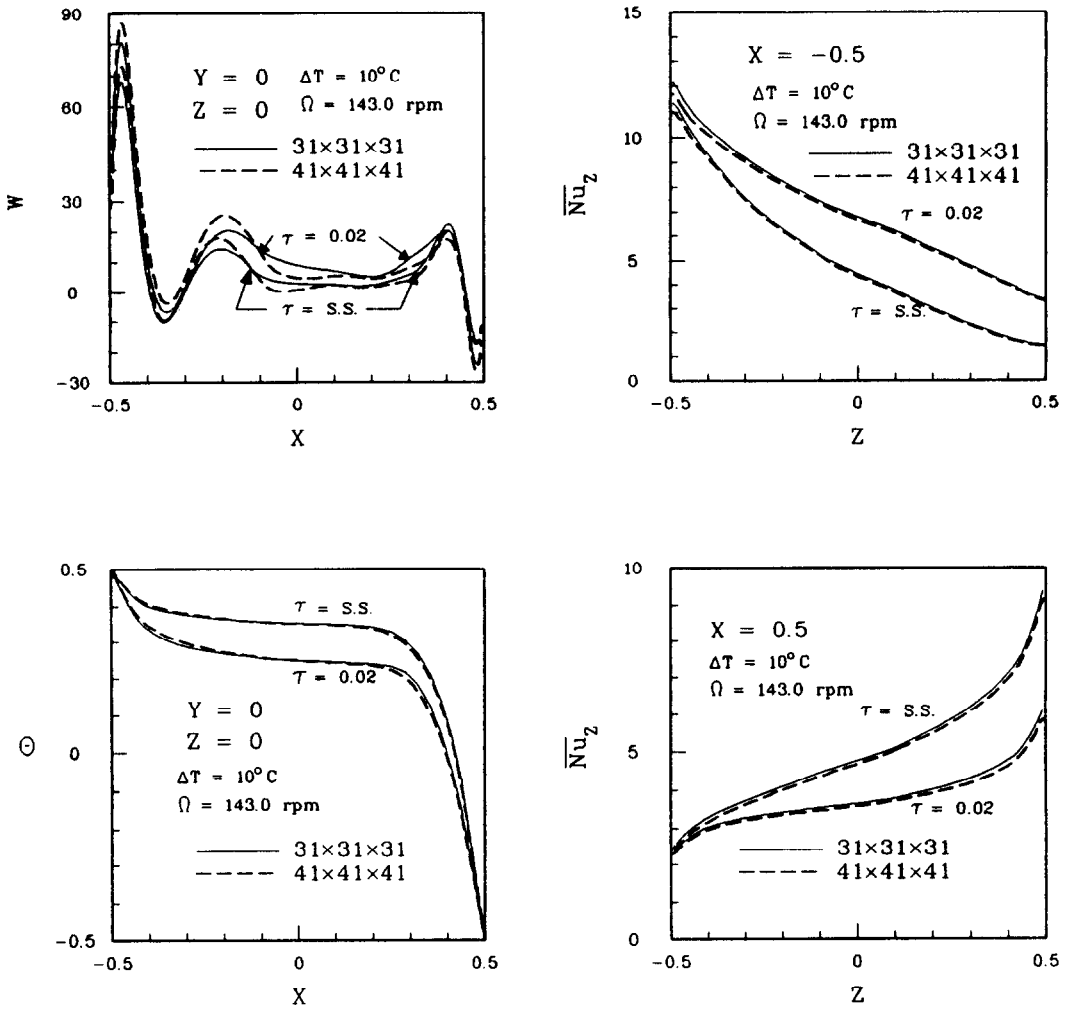

Fig. 2. Comparison of the numerically predicted velocity and temperature profiles along the X-direction at line $Y = 0$ and $Z = 0$ and the Y-direction averaged Nusselt number calculated from two different grids for $\Delta T = 10°C$, $\phi = 0°$ and $\Omega = 143$ rpm at two time instants.

agreement. To exemplify this comparison, results for a case with $\Omega = 143$ rpm, $\Delta T = 10°C$ and $\phi = 0°$ are shown in Fig. 2. Good agreement is noted in the velocity and temperature profiles computed from the two different grids over the entire transients. Through these tests, the proposed numerical method is considered to be suitable for the present problem.

3. EXPERIMENTAL APPARATUS FOR TEMPERATURE MEASUREMENT

The experimental system for measuring the thermal characteristics in a rotating air cavity schematically shown in Fig. 3 consists of four parts—rotating frame, test section, temperature control unit and temperature measuring unit. Figure 4 shows the details of the test section.

The rotating frame is made up of a rotary table of 31.5 cm in diameter and is mounted on a steel shaft of 3 cm in diameter. The frame is designed to provide a space of 27.6 cm in diameter and 27.3 cm in height for housing the test section. The shaft is rotated by a 2 horse power d.c. motor with its speed controlled by an inverter. Besides, the rotating speed is detected by a photo-electric tachometer. Care is taken to ensure that the table rotates centrally and steadily.

The test section fixed on the rotating table is a cubic air enclosure of 10 cm in length. Two opposite walls of the cavity made of 2.5 mm thick copper plates were controlled at uniform, but different temperatures by circulating constant temperature coolants through them. Two fluid sliprings were used to allow the coolants to pass from the stationary thermostats to the rotating cavity. The thermostats used are the LAUDA RK-20 compact constant temperature baths with a temperature range of −40–150°C and a resolution of 0.1°C. Care must be taken to prevent the coolant leak from the fluid sliprings. The other walls were made of 10 mm thick acrylic plates and were thermally insulated by the super-lon foam. Through this arrange-

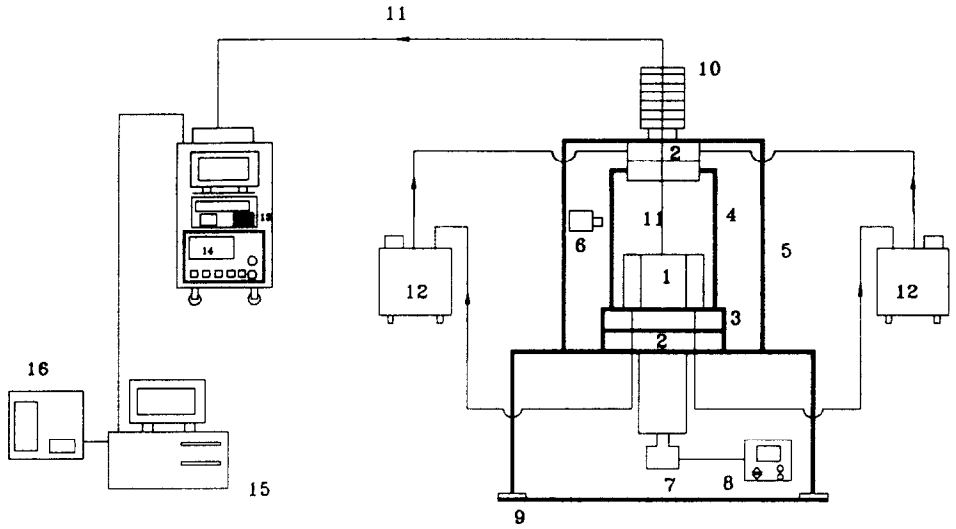

1 : test section
2 : fluid slip ring
3 : supporting frame
4 : rotating frame
5 : statatic frame
6 : photo – electric tachometer
7 : 2 Hp induction motor
8 : inverter
9 : platform
10 : slip ring
11 : thermocouples
12 : thermostat
13 : data acquisition system
14 : digital multimeter
15 : P.C. computer
16 : laser printer

Fig. 3. Schematic diagram of the experimental system.

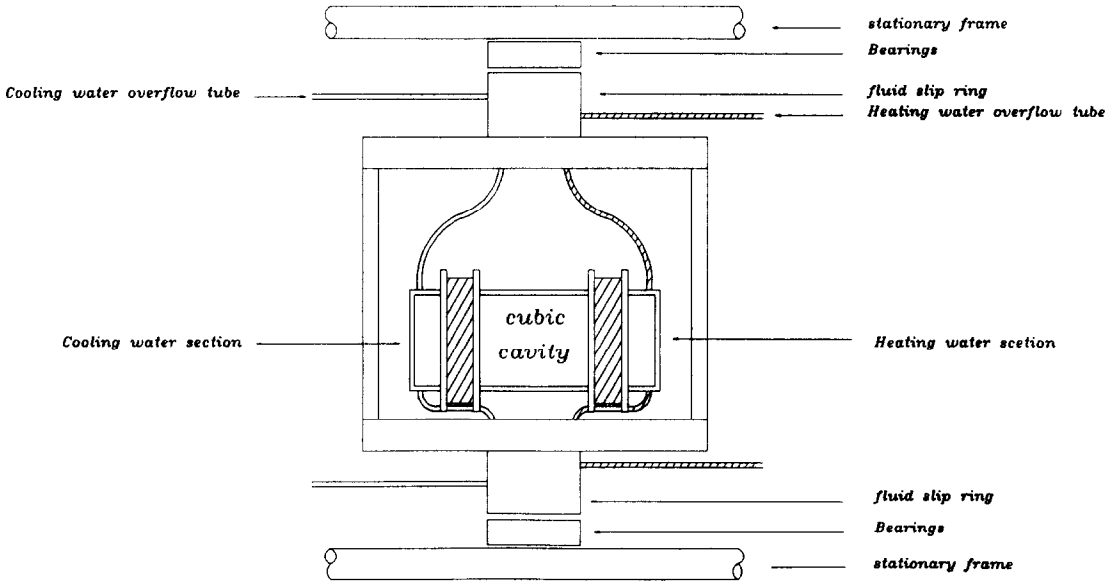

Fig. 4. Rotating assembly.

Table 1. Uniformity of the isothermal walls

Location (X, Y, Z)	T_L [°C]	Location (X, Y, Z)	T_H [°C]
0.5, 0.355, −0.355	15.05	−0.5, −0.355, −0.355	35.07
0.5, 0.0, −0.355	15.04	−0.5, 0.0, −0.355	35.15
0.5, −0.355, −0.355	15.02	−0.5, 0.355, −0.355	35.14
0.5, 0.355, 0.0	15.04	−0.5, −0.355, 0.0	35.09
0.5, 0.0, 0.0	15.00	−0.5, 0.0, 0.0	35.13
0.5, −0.355, 0.0	15.01	−0.5, 0.355, 0.0	35.10
0.5, 0.355, 0.355	14.92	−0.5, −0.355, 0.355	34.98
0.5, 0.0, 0.355	14.95	−0.5, 0.0, 0.355	35.02
0.5, −0.355, 0.355	14.90	−0.5, 0.355, 0.355	35.00

ment the temperature uniformity of the isothermal plates can be controlled to within ±0.1°C. The sampled measured data for the temperature of the hot and cold walls at selected locations are given in Table 1.

The temporal and spatial variations of the air temperature in the rotating cavity were measured by directly inserting thermocouples of T-type into the cavity. The thermocouples are fixed at the designated locations by the high performance fine Neoflon thread, which is in turn fixed across a pair of opposite side walls. Prior to installation the thermocouples were calibrated by the LAUDA thermostats and high precision liquid-in-glass thermometers. The voltage signals from the thermocouples were passed through a slip ring to the HP 3852 A data acquisition/control system and then to a personal computer for further data processing. Data collection is normally started when the flow already reaches steady or statistical state. In view of the flow being at low speed and the cavity being rotated, velocity measurement is difficult and is not conducted here.

The test was started by first setting the temperatures of the thermostats at the predetermined values and then recirculating the coolants through the isothermal walls of the rotating cavity. The mean value of the hot and cold plate temperatures was chosen to be equal to the ambient temperature, so that the heat loss from the cavity to the ambient can be reduced. In the meantime the cavity was rotated at the predetermined speed. Then the temperature of the air inside the cavity was measured at selected locations. After the transient stage has elapsed, the data for the steady or statistical state were sorted and analyzed.

The ranges of the governing parameters to be investigated are as follows: the rotating speed varied from 0 to 453 rpm, the inclined angle from 0° to 75° and the temperature difference across the cavity from 2 to 10°C for a cavity of $10 \times 10 \times 10$ cm^3. The uncertainty analysis of the measurement was summarized in Table 2.

4. RESULTS AND DISCUSSION

In the following only a small sample of the results from the present study will be presented here to illustrate the flow and thermal characteristics in an air cavity rotating at various rotation rates and subject to various temperature differences across a pair of opposite side walls.

4.1. *Flow structures at various rotation rates in vertical cavity*

For comparison purpose the numerically predicted steady thermal and flow structures for the limiting case of the nonrotating cavity ($\Omega = 0$) with $Ra = 9.43 \times 10^5$ (or $\Delta T = 10$°C and $H = 10$ cm) and $\phi = 0°$ are given in Fig. 5 in which the velocity vector maps and isotherms in selected planes from the front, side and top views are plotted. The flow for this case is centrosymmetric and is characterized by a strong recirculation rising from the hot plate and sinking near the cold plate with weak recirculation near the vertical central plane parallel to the isothermal walls at $X = 0$ and near the horizontal middle plane at $Z = 0$, as evident from the front and top views (Fig. 5). Thermal boundary layers exist in the regions near the hot and cold walls and stable thermal stratification prevails in the cavity core. Complete details of the flow in a stationary cavity can be found in our earlier study [28]. Now as the cavity is rotated at 30.7 rpm with other parameters fixed at the same values as the previous case, the resulting steady flow from the numerical computation is shown in Fig. 6. Contrasting these results with those in Fig. 5 for the nonrotating cavity indicates that at this rotation rate the

Table 2. Summary of uncertainty analysis

Parameters	Uncertainty
H (m)	±0.0005 m
T_H, T_L	±0.1°C (non-rotating)
T_H, T_L	±0.2°C (rotating)
T (Thermocouples)	±0.05°C
α (m^2 s^{-1})	±0.07%
β (K^{-1})	±0.05%
ρ_0 (kg m^{-3})	±0.05%
ν (m^2 s^{-1})	±0.07%
Ω (rpm)	±0.3%
ϕ (degree)	±0.5°
Ta	±10.5%
Ra	±2.5%
Ra_w	±11.5%

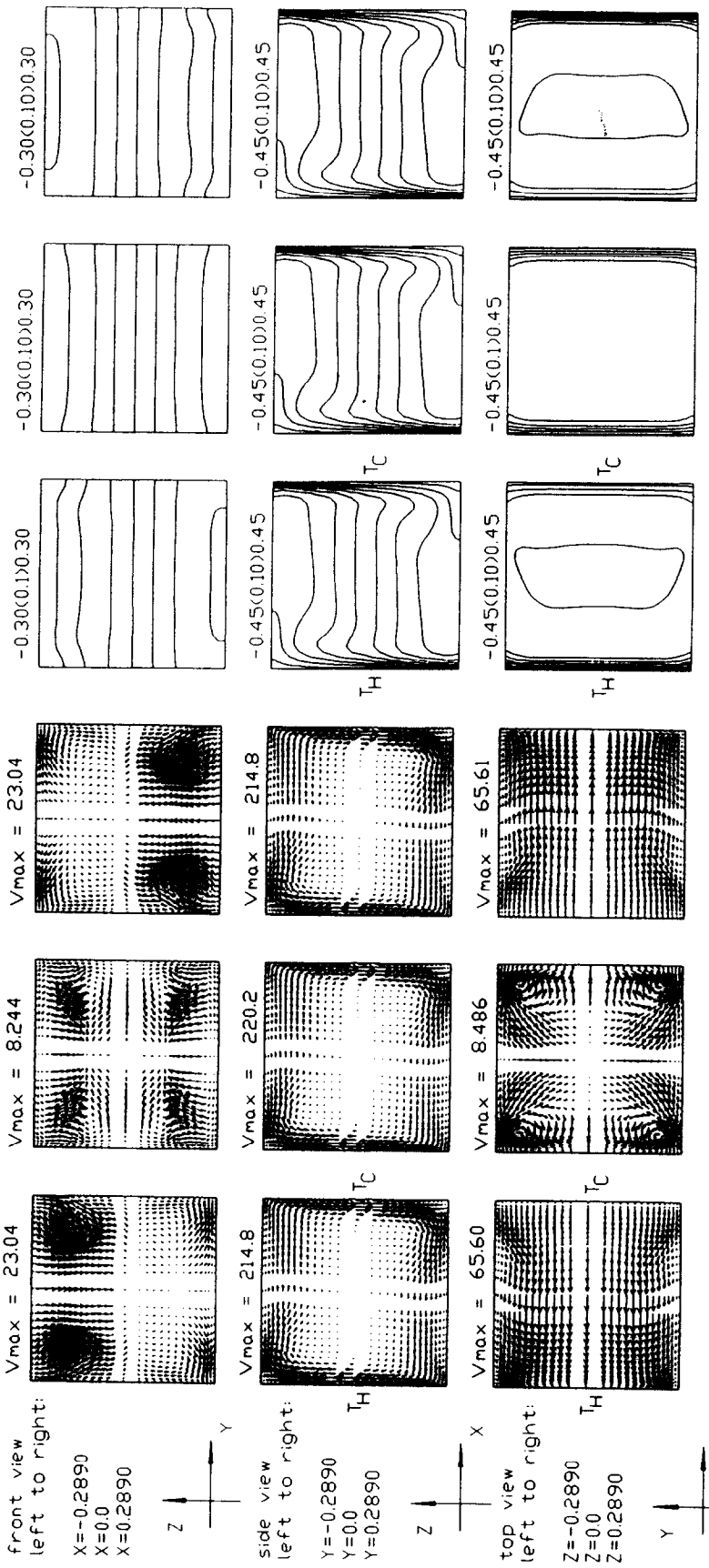

Fig. 5. The velocity vector maps (a) and isotherms (b) in selected planes for $\phi = 0°$, $\Delta T = 10°C$ and $\Omega = 0$ rpm at steady state ($Ra = 9.43 \times 10^5$, $Ta = 0$, $Ra_w = 0$, $\phi = 0°$).

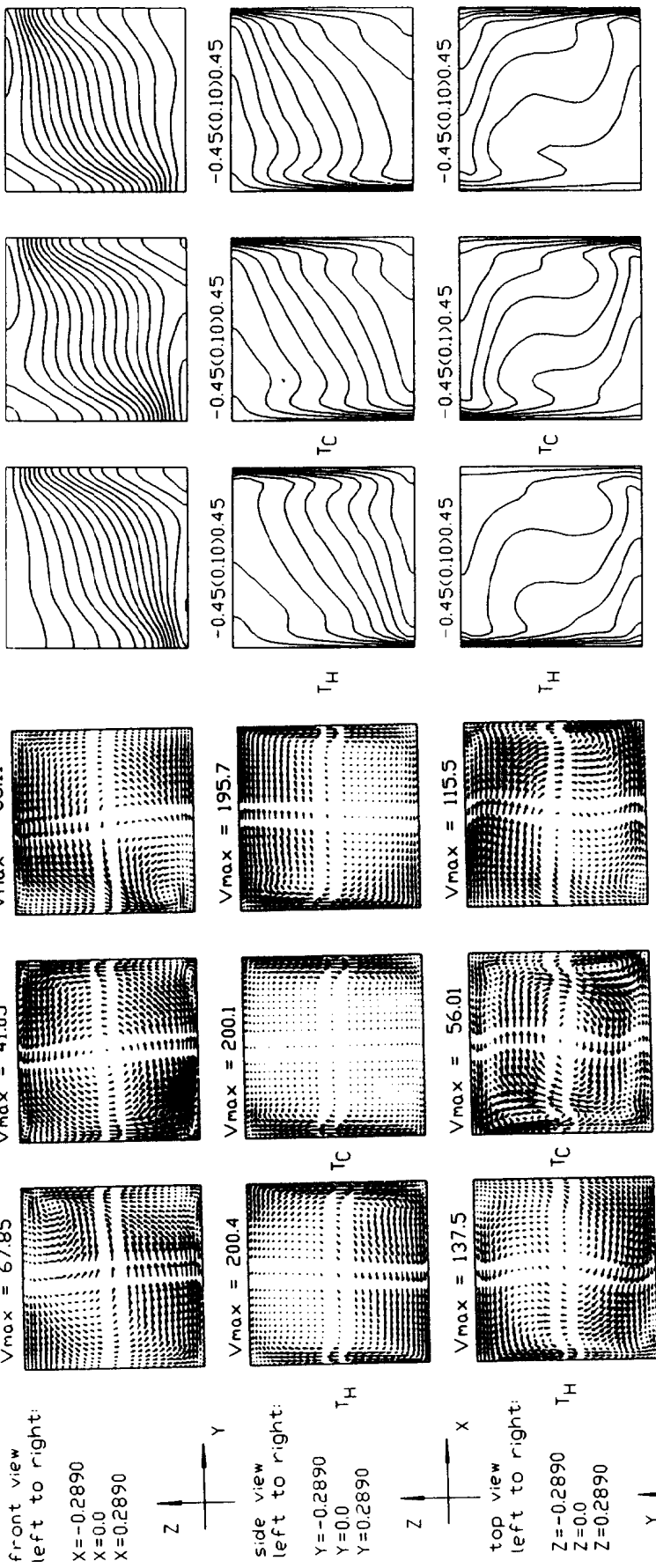

Fig. 6. The velocity vector maps (a) and isotherms (b) in selected planes for $\phi = 0°$, $\Delta T = 10°C$ and $\Omega = 30.7$ rpm at steady state ($Ra = 9.43 \times 10^5$, $Ta = 4.62 \times 10^6$, $Ra_w = 10^5$, $\phi = 0°$).

main flow, clearly seen from the side view, is weakened to a certain degree by the cavity rotation with the accompanying much stronger flow recirculation in the horizontal planes (top view) and in the planes parallel with the hot plate (front view). This speedup of the cross plane secondary flow modifies the temperature contours significantly [Fig. 6(b)]. The core flow is no longer thermally stably stratified. This significant flow modification at this low rotation rate can be understood by checking the governing dimensionless groups corresponding to this case. The values of the parameters for this case are $Ra = 9.43 \times 10^5$, $Ta = 4.62 \times 10^6$ and $Ra_w = 10^5$. Hence, the Coriolis force (Taylor number) is so high that it exerts an important effect on the thermal buoyancy driven flow [1]. Moreover, the flow is no longer centrosymmetric for this case. Raising the rotation rate from 30.7 rpm to 97.4 rpm with ΔT still fixed at 10°C results in the increase in the Ta and Ra_w by 10 times, and thus we have $Ra = 9.43 \times 10^5$, $Ta = 4.62 \times 10^7$ and $Ra_w = 10^6$. The numerically predicted steady flow and temperature fields for this case shown in Fig. 7 indicate that the driven flow does not close to that driven by the thermal buoyancy, rotational buoyancy or Coriolis force alone [1], although the flow structure viewing from the top possesses some characteristics of the centrifugal force dominated flow, which is characterized by a pair of vertical vortex rolls. This is conjectured to be the consequence of the comparable magnitude of the Ra, Ra_w and Ta in the flow and there are strong interactions among them. Also note that at this higher rotation rate the flow is significantly suppressed, as evident from comparing Figs. 6 and 7. Results were also obtained for $H = 10$ cm and $\Delta T = 4.6$°C and 2°C at various rotation rates. A similar trend was noted from these results.

4.2. *Effects of rotation rate on the velocity and temperature profiles*

The numerically predicted deceleration of the main recirculation of the thermal buoyancy driven flow, and the thickening of the velocity and thermal boundary layers on the hot and cold walls by the cavity rotation, are illustrated by examining the steady vertical velocity and temperature profiles on a horizontal line at $Y = 0$ and $Z = 0$ at the midheight of the cavity given in Fig. 8 for $\Delta T = 10$°C and 4.6°C for various Ω. The measured data for the air temperature from the present study are also included in the plots. Larger flow slowdown by the higher rotation rate is clearly seen from these results. The gradual disappearance of the dips in the temperature profiles at increasing rotation rate is also observed. The calculated temperature profiles agree reasonably with the measured data, except at high rotation rates, $\Omega = 97.4$ rpm and 143 rpm. At these high rotation rates the numerical simulation overpredicted the temperature.

4.3. *Average Nusselt numbers*

The numerically predicted Y-direction average Nusselt numbers $\overline{Nu}_z$ on the hot and cold walls are presented in Fig. 9 for $\Delta T = 10$°C and 4.6°C for $\phi = 0°$ at various rotation rates. The results clearly show the reduction of convective heat transfer from the walls to the air by the cavity rotation especially in the high heat transfer regions near the leading edges of the boundary layers on the isothermal walls. At high rotation rates the heat transfer near the upper left and lower right corners of the cavity can be slightly enhanced by the rotation.

Finally, the numerically computed space-average Nusselt numbers $\overline{Nu}$ on the isothermal walls at various Ω are displayed in Fig. 10 for $\Delta T = 10$°C and 4.6°C for $\phi = 0°$. The results suggest that at low rotation rate ($\Omega < 50$ rpm) significant heat transfer reduction by the cavity rotation occurs, but at high rotation rate ($\Omega > 100$ rpm) rotating the cavity does not further reduce the heat transfer for $\Delta T = 10$°C. In fact, a slight increase in $\overline{Nu}$ may result from raising the rotation rate over 100 rpm.

4.4. *Rotation induced flow stabilization or destabilization*

In the present study the stabilizing or destabilizing effect of the buoyancy driven flow by the cavity rotation are investigated by examining the time variations of the measured air temperature at selected locations in the cavity. Only the long term results are studied at which the temperature already reaches steady or statistical state.

Results are first presented for the vertical cavity ($\phi = 0°$). When the cavity is stationary ($\Omega = 0$) the thermal buoyancy driven flow is found to be as steady after initially being transient for all the cases studied ($\Delta T \leqslant 10$°C), as those from the numerical simulation [28]. Rotating the cavity was found to destabilize the flow when the rotation speed exceeds a certain critical value. Figure 11 shows the sampled data for the time records of the air temperature at various rotation rates at location $X = 0.42$, $Y = 0$ and $Z = 0$ for $\Delta T = 10$°C and 4.6°C ($Ra = 9.43 \times 10^5$ and 4.36×10^5). These results clearly suggest that for $\Delta T = 10$°C the flow is steady at $\Omega < 80$ rpm. At this low rotation speed, random oscillations at very small amplitude due to background disturbances are noted. Small amplitude periodic temperature oscillation was detected at $\Omega = 97.4$ rpm. At $\Omega = 143$ rpm, high frequency small amplitude oscillation superimposes on the periodic part. The temperature oscillation becomes somewhat irregular and in higher amplitude at $\Omega = 308$ and 453 rpm. Similar trend was noted for $\Delta T = 4.6$°C [Fig. 11(b)], except that the destabilization is initiated at a lower Ω and the oscillation amplitude is larger.

Checking the time histories of the air temperature at five different locations in Fig. 12 for $\Omega = 97.4$ rpm for $\Delta T = 10$ and 4.6°C reveals that the air temperature at these locations oscillates at nearly the same frequency, but in different amplitudes. Closer to the hot wall a slightly smaller temperature oscillation is noted. The measured data for a rotating inclined cavity with $\phi = 30°$ and 60° also manifest that at small

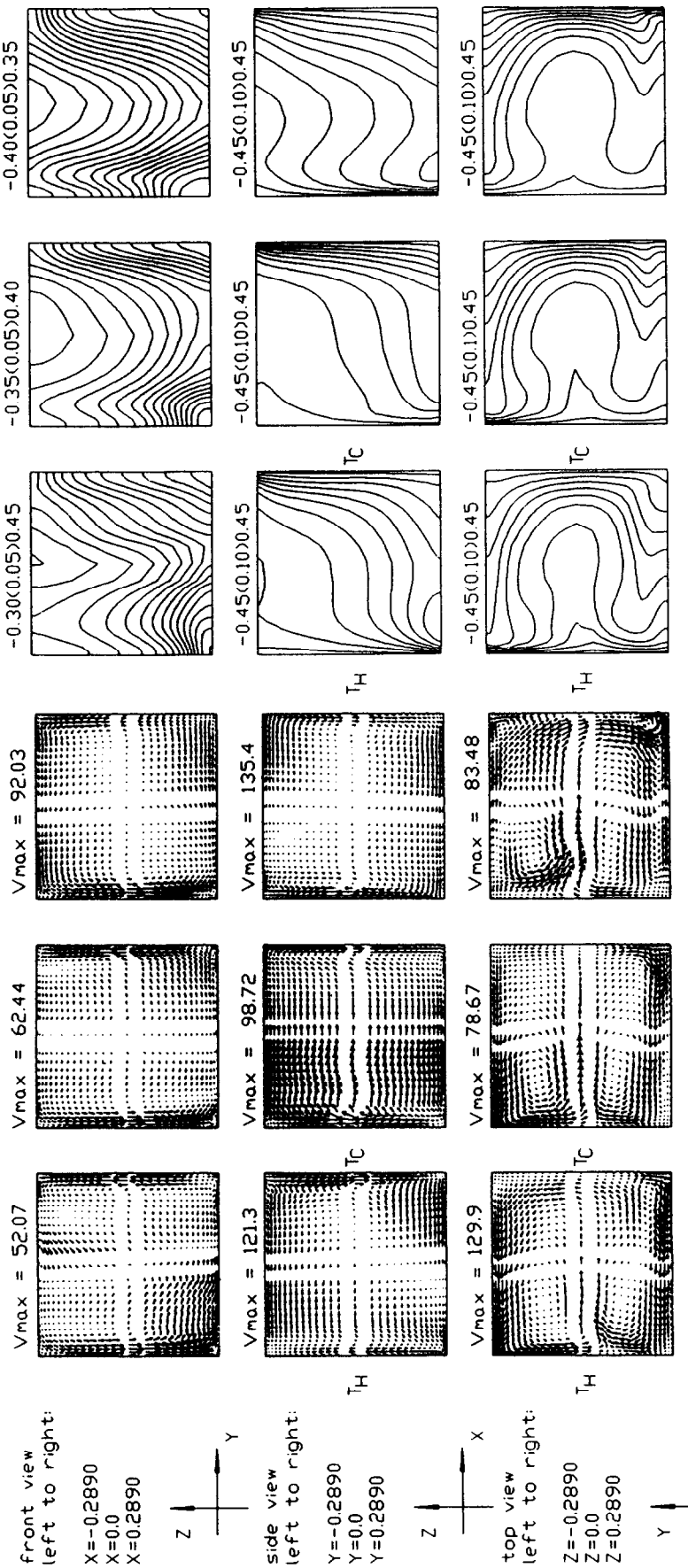

Fig. 7. The velocity vector maps (a) and isotherms (b) in selected planes for $\phi = 0°$, $\Delta T = 10°C$ and $\Omega = 97.4$ rpm at steady state ($Ra = 9.43 \times 10^5$, $Ta = 4.62 \times 10^7$, $Ra_w = 10^6$, $\phi = 0°$).

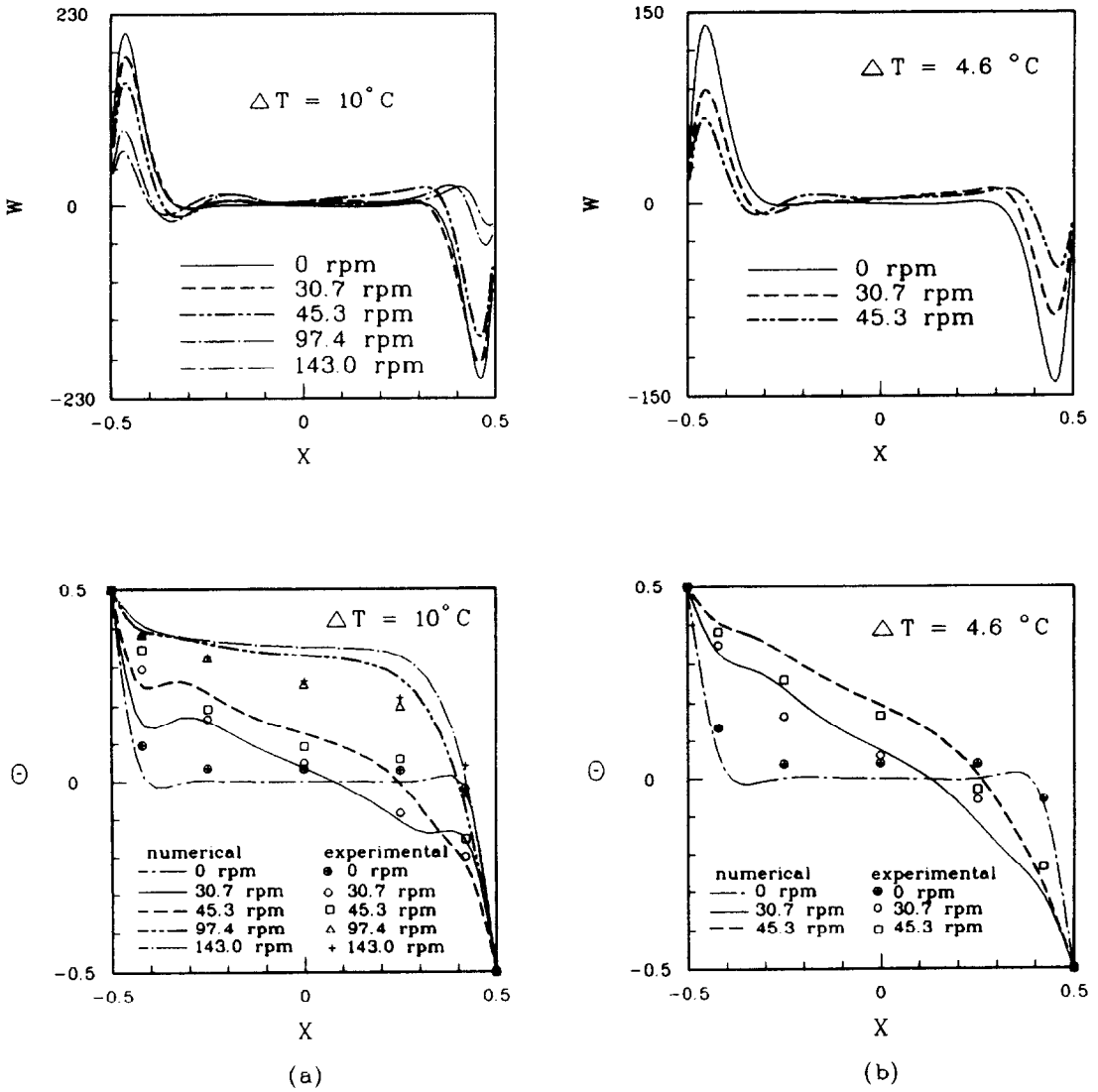

Fig. 8. Vertical velocity and temperature distributions along the X-direction on the line $Y = 0$, $Z = 0$ for $\phi = 0°$, at (a) $\Delta T = 10°C$ and (b) $\Delta T = 4.6°C$ at different rotating speeds.

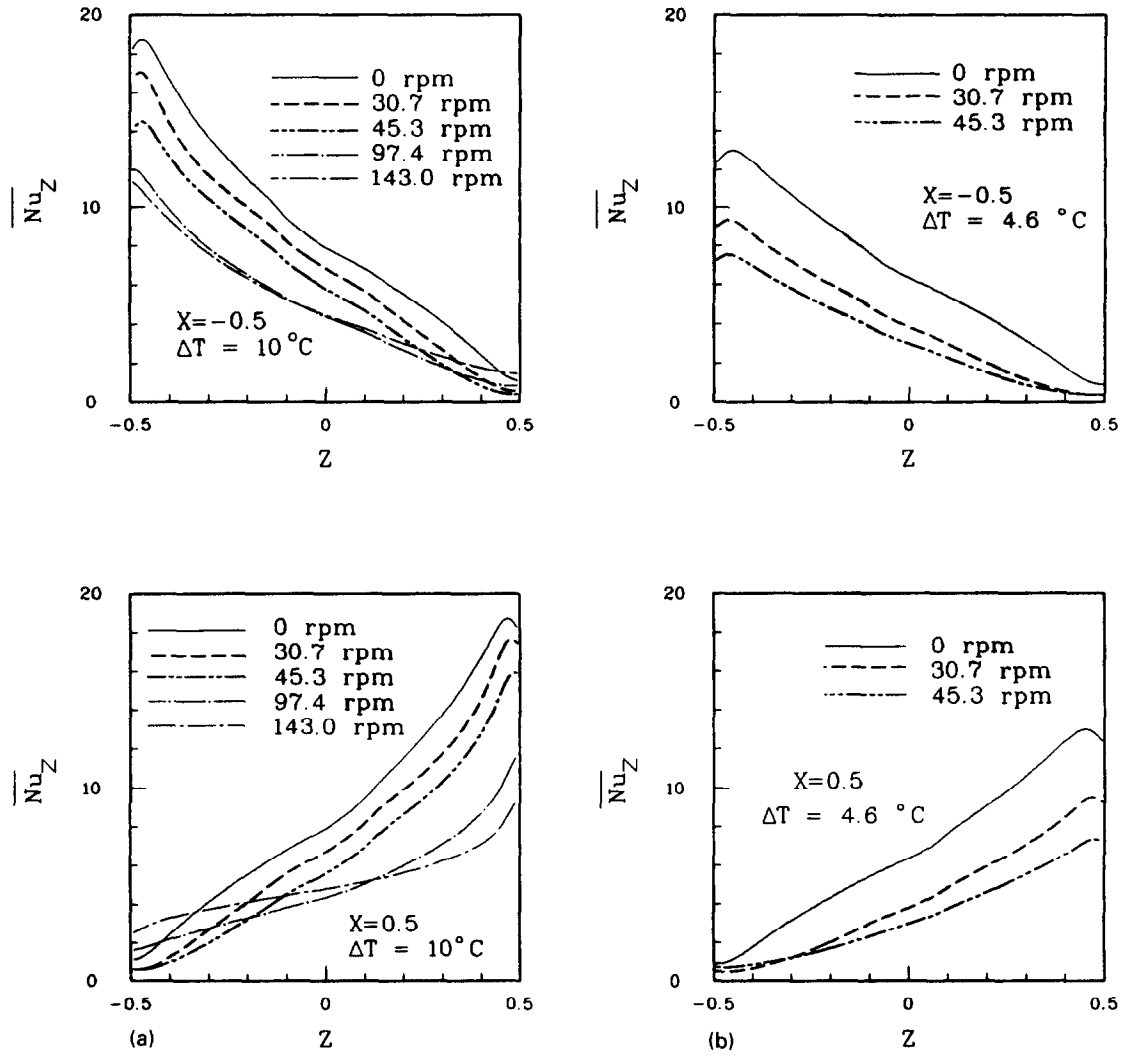

Fig. 9. Y-direction average Nusselt number distributions on the hot and cold walls for $\phi = 0°$ at (a) $\Delta T = 10°C$ and (b) $\Delta T = 4.6°C$ at different rotation speeds.

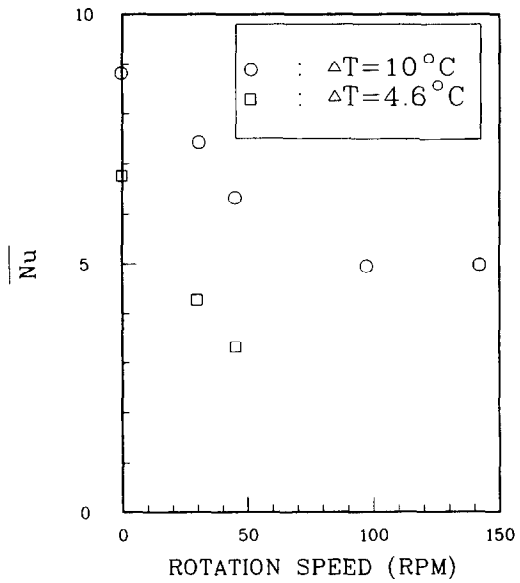

Fig. 10. Space average Nusselt number for $\phi = 0°$ at different temperature gradients and rotating speeds.

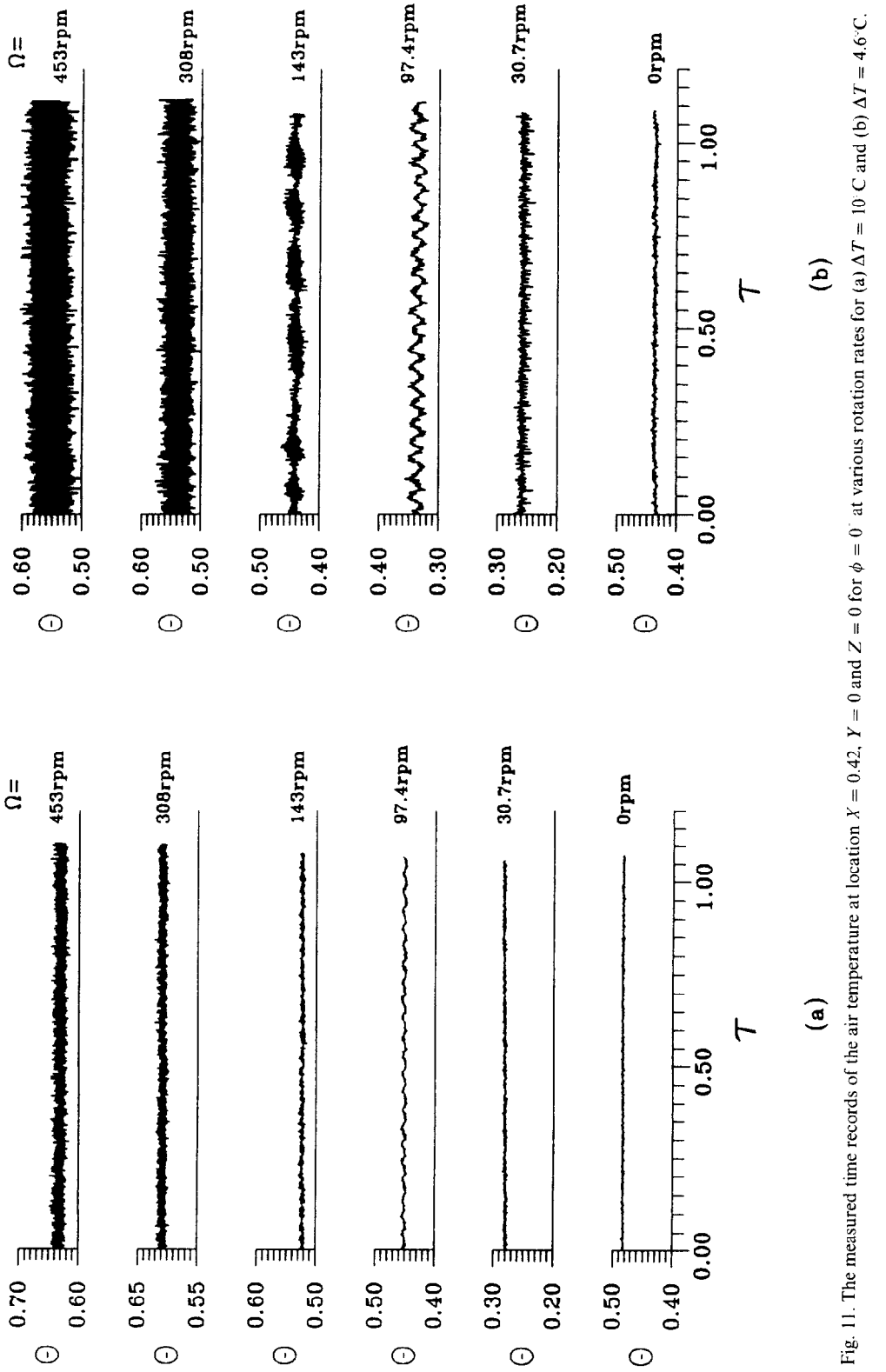

Fig. 11. The measured time records of the air temperature at location $X = 0.42$, $Y = 0$ and $Z = 0$ for $\phi = 0^{\circ}$ at various rotation rates for (a) $\Delta T = 10^{\circ}$C and (b) $\Delta T = 4.6^{\circ}$C.

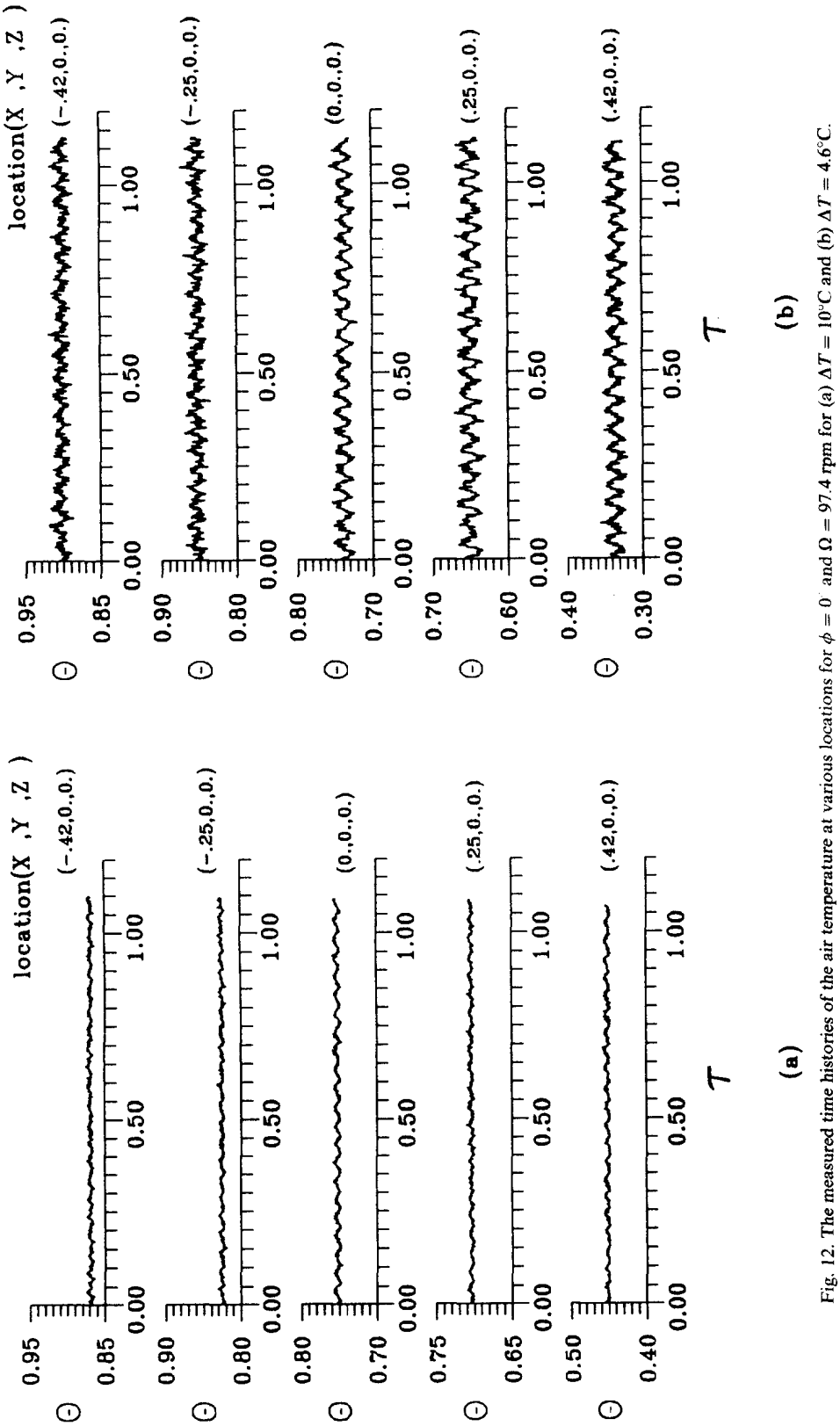

Fig. 12. The measured time histories of the air temperature at various locations for $\phi = 0^{\circ}$ and $\Omega = 97.4$ rpm for (a) $\Delta T = 10^{\circ}$C and (b) $\Delta T = 4.6^{\circ}$C.

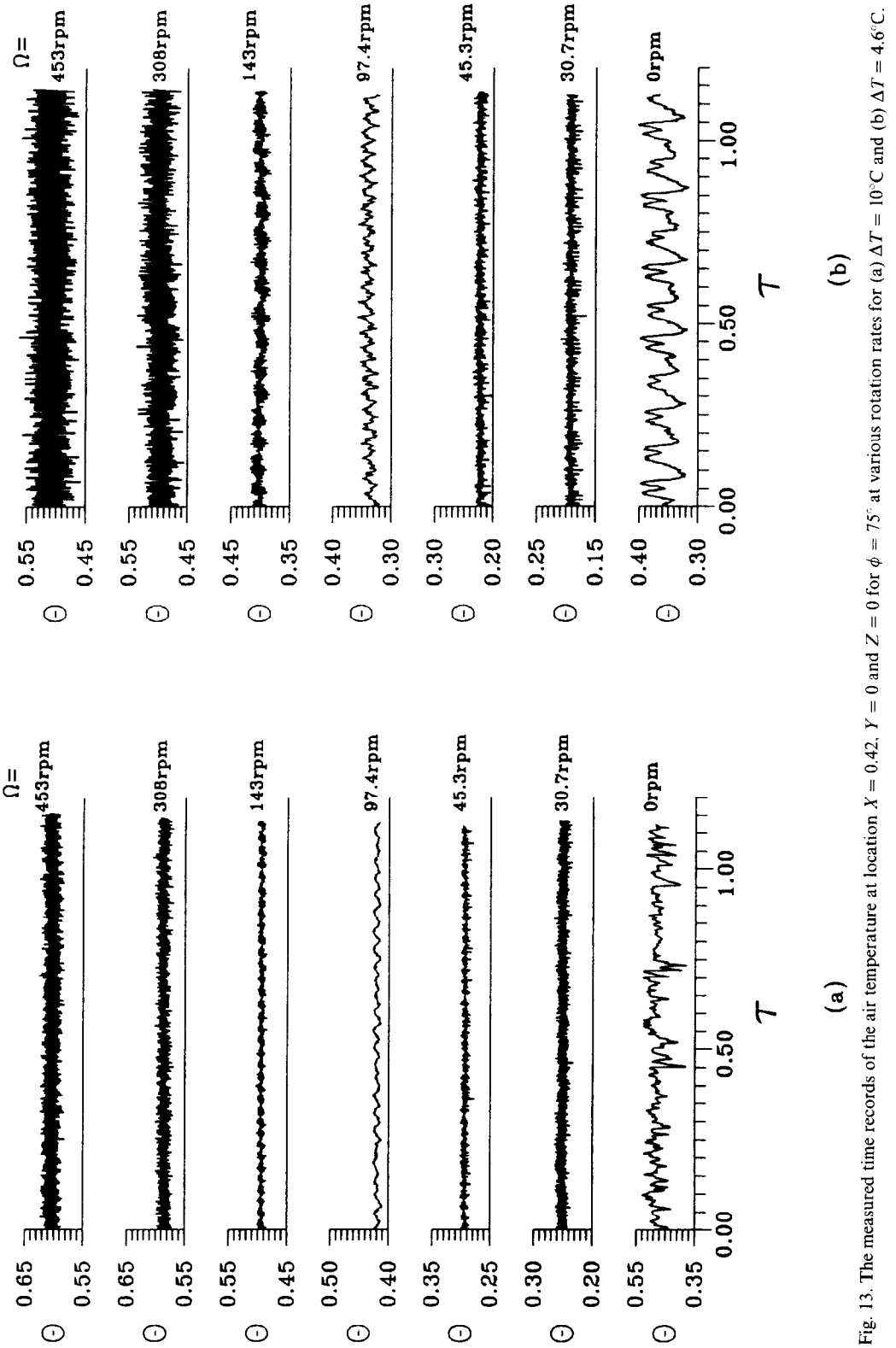

Fig. 13. The measured time records of the air temperature at location $X = 0.42$, $Y = 0$ and $Z = 0$ for $\phi = 75^{\circ}$ at various rotation rates for (a) $\Delta T = 10^{\circ}$C and (b) $\Delta T = 4.6^{\circ}$C.

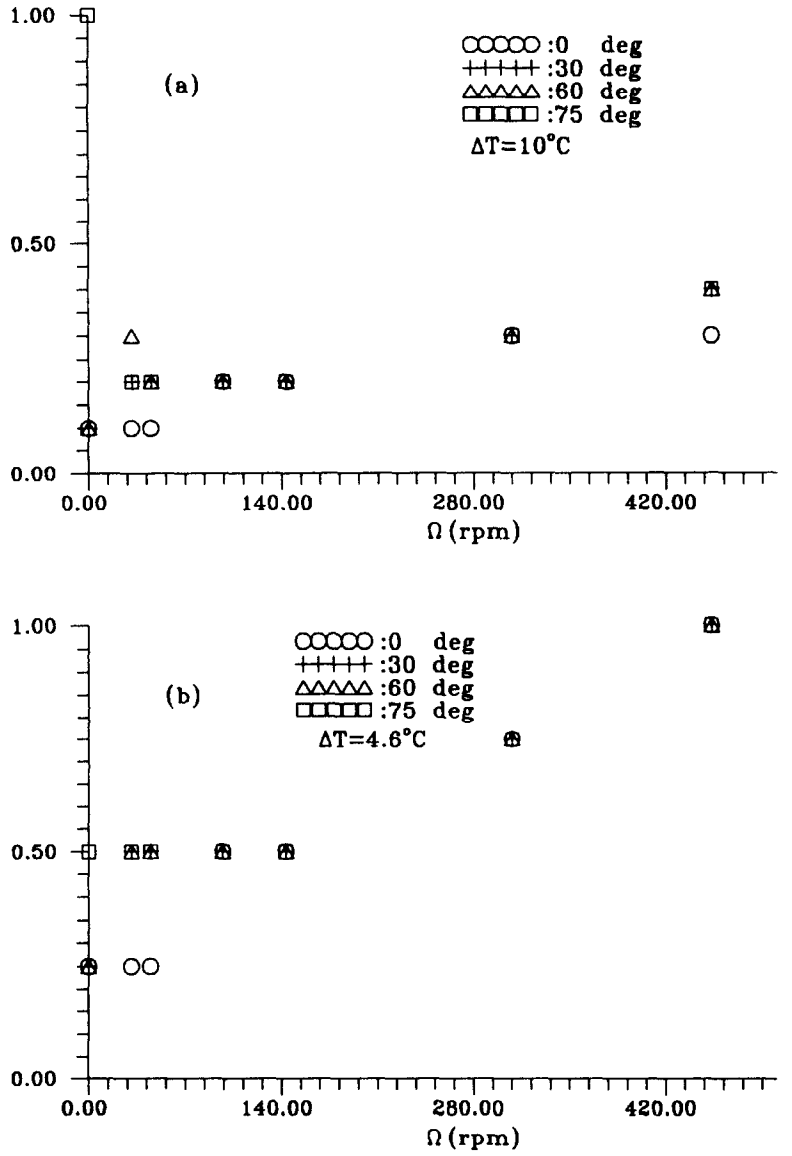

Fig. 14. The normalized temperature oscillation amplitude for various rotation rates and inclined angles.

rotation rate steady temperature field prevails, but the air temperature becomes time oscillatory for Ω exceeding certain value, which depends on the inclined angle.

At a higher inclined angle of 75° the resulting flow in a nonrotating cavity ($\Omega = 0$) is time oscillatory at larger τ for $\Delta T = 10$°C and 4.6°C. Rotating the cavity is found to yield stabilizing effects on the flow. Specifically the flow oscillation is damped out or suppressed to a smaller amplitude by the cavity rotation, as illustrated by the data in Fig. 13. Note that at $\Delta T = 10$°C, a large amplitude irregular temperature fluctuation is detected for $\Omega = 0$. At low rotation speed of 30.7 and 45.3 rpm the amplitude of the oscillation is much smaller. The temperature oscillation is nearly time periodic at $\Omega = 97.4$ rpm. At higher Ω (= 143 and 308 rpm) small amplitude irregular oscillation prevails. Finally, it is also noted from the results that at a higher rotation speed of 453 rpm ($Ta = 10^9$ and $Ra_w = 2.16 \times 10^7$), the flow is destabilized by the cavity rotation with the oscillation amplitude increased noticeably. A similar trend is noted from the data in Fig. 13(b) for $\Delta T = 4.6$°C, except that the oscillation amplitude is larger. The above results from the experimental measurement clearly indicate that rotating the cavity does not always produce stabilizing effects on the flow.

The measured data from the present study for the oscillation amplitude of the air temperature δT at the location (0.42, 0, 0) for various ϕ and Ω when normalized by δT_0 that is the amplitude of the temperature oscillation for $\phi = 75°$ and $\Omega = 0$ rpm are

presented in Fig. 14 for $\Delta T = 10$ and 4.6°C. The effects of the cavity rotation on the flow stability are clearly seen from these results.

5. CONCLUDING REMARKS

Through a combined direct three-dimensional numerical simulation and experimental measurement, the flow structure and its stability in a differentially heated rotating cavity of air were investigated. The numerical prediction clearly revealed the complex multicellular recirculating flow driven by the simultaneous interactions of the thermal buoyancy and the centrifugal and Coriolis forces. Besides, significant flow deceleration and heat transfer reduction only occur at low rotation rate. The present experimental data suggested that rotating the cavity results in flow stabilization at low rotation speed. The flow can be destabilized when the cavity is in fast rotation.

During the course of this investigation it is realized that the effects of the cavity rotation on the flow stability are particularly important for the cavity flow of the liquid metal, which is the material for manufacturing the single wafer for the semiconductor industry. A detailed study on the stability of the rotating cavity flow of a low Prandtl number liquid metal is rather important and requires exhaustive exploration.

Acknowledgement—The financial support of this study by the engineering division of National Science Council of Taiwan, Republic of China through the contract NSC 81-0401 E-009-548 is greatly appreciated. The support of the present computation by the National Center for The High-Performance computing and by the computer center of the national Chiao Tung University, Taiwan, Republic of China is also acknowledged.

REFERENCES

1. T. L. Lee and T. F. Lin, Transient three-dimensional convection of air in a differentially heated rotating cubic cavity, *Int. J. Heat Mass Transfer* **39,** 1243–1255 (1996).
2. P. P. Niller and F. E. Bisshopp, On the influence of Coriolis force on onset of thermal convection, *J. Fluid Mech.* **22,** 753–761 (1965).
3. George Veronis, Large-amplitude Bénard convection in a rotating fluid, *J. Fluid Mech.* **31,** 113–139 (1968).
4. G. Küppers and D. Lortz, Transition from laminar convection to thermal turbulence in a rotating fluid layer, *J. Fluid Mech.* **35,** 609–620 (1969).
5. H. T. Rossby, A study of Bénard convection with and without rotation, *J. Fluid Mech.* **36,** 309–335 (1969).
6. C. Hunter and N. Riahi, Nonlinear convection in a rotating fluid, *J. Fluid Mech.* **72,** 433–454 (1975).
7. N. Rudraiah and O. P. Chandna, Effects of Coriolis force and nonuniform temperature gradient on the Rayleigh–Bénard convection, *Can. J. Phys.* **64,** 90–99 (1986).
8. R. M. Clever and F. H. Busse, Nonlinear properties of convection rolls in a horizontal layer rotating about a vertical axis, *J. Fluid Mech.* **94,** 609–627 (1979).
9. J. L. Hudson, D. Tang and S. Abell, Experiments on centrifugal driven thermal convection in a rotating cylinder, *J. Fluid Mech.* **86,** 147–159 (1978).
10. D. Tang and J. L. Hudson, Experiments on a rotating fluid heated from below, *Int. J. Heat Mass Transfer* **26,** 943–949 (1983).
11. J. W. Chew, Computation of convective laminar flow in rotating cavities. *J. Fluid Mech.* **153,** 339–360 (1985).
12. J. C. Buell and I. Catton, Effect of rotation on the stability of a bounded cylindrical layer of fluid heated from below, *Phys. Fluids* **26,** 892–896 (1983).
13. J. M. Pfotenhauer, J. J. Niemela and R. J. Donnelly, Stability and heat transfer of rotating criogens. Part 3. Effects of finite cylindrical geometry and rotation on the onset of convection, *J. Fluid Mech.* **175,** 85–96 (1987).
14. B. M. Boubnov and G. S. Golitsyn, Experimental study of convective structures in rotating fluid, *J. Fluid Mech.* **167,** 503–531 (1986).
15. A. G. Kirdyashkin and V. E. Distonov, Hydrodynamics and heat transfer in a vertical cylinder exposed to periodically varying centrifugal forces (accelerated crucible-rotation technique), *Int. J. Heat Mass Transfer* **33,** 1397–1415 (1990).
16. S. Abell and J. L. Hudson, An experimental study of centrifugally driven free convection in rectangular cavity, *Int. J. Heat Mass Transfer* **18,** 1415–1423 (1975).
17. D. H. Hathaway and R. C. J. Somerville, Three-dimensional simulations of convection in layers with tilted rotation vectors, *J. Fluid Mech.* **126,** 75–89 (1983).
18. K. Bühler and H. Oertel, Thermal cellular convection in rotating rectangular boxes, *J. Fluid Mech.* **114,** 261–282 (1982).
19. S. A. Condie and R. W. Griffiths, Convection in rotating cavity: modeling ocean circulation, *J. Fluid Mech.* **207,** 453–474 (1989).
20. G. M. Homsy and J. L. Hudson, Centrifugally driven thermal convection in a rotating cylinder, *J. Fluid Mech.* **35,** 33–52 (1969).
21. S. V. Patankar, *Numerical Heat Transfer and Fluid Flow*, pp. 90–92 Hemisphere, Washington, DC (1980).
22. M. Fortin, R. Peyret and R. Temam, *Lecture Notes in Physics* Vol. 8, pp. 337–342. Springer, New York (1971).
23. F. Bauman, A. Gadgil, R. Kammerud and R. Greif, *Buoyancy-Driven Convection in Rectangular Enclosures: Experimental Results and Numerical Calculations.* ASME publication 80-HT-66, (1980).
24. G. De Vahl Davis, Laminar natural convection in an enclosed rectangular cavity, *Int. J. Heat Mass Transfer* **11,** 1675–1693 (1968).
25. S. M. Bajorek and J. R. Lloyd, Experimental investigation of natural convection in partitioned enclosures, *J. Heat Transfer* **104,** 527–532 (1982).
26. F. Hamady, Experimental study of local natural convection heat transfer in inclined and rotating enclosures, Ph.D. Dissertation, Michigan State University (1987).
27. T. Fusegj, J. M. Hyun, K. Kuwahara and B. Farouk, A numerical study of three-dimensional natural convection in a differentially heated cubical enclosure, *Int. J. Heat Transfer* **34,** 1543–1557 (1991).
28. T. L. Lee and T. F. Lin, Three-dimensional natural convection of air in an inclined cubic cavity, *Numer. Heat Transfer* **27,** 681–703 (1995).